Li *et al.*
Chinese Journal of Mechanical Engineering (2022) 35:30
https://doi.org/10.1186/s10033-022-00691-7

Chinese Journal of Mechanical Engineering

ORIGINAL ARTICLE

Open Access

Theoretical Analysis and Experimental Research of Surface Texture Hydrodynamic Lubrication

Dan Li[1,3], Xuefeng Yang[1*], Yuanbo Wu[1], Jian Cheng[2], Shouren Wang[1], Zhuang Wan[1], Wenbo Liu[1] and Guofeng Xia[1]

Abstract

The research on surface texture is developing from single macro-texture to composite micro-nano texture. The current research on the anti-friction mechanism and theoretical models of textures is relatively weak. Studying the characteristics of different types of surface textures and determining the applicable working conditions of each texture is the focus of current research. In this paper, a mathematical model of hydrodynamic lubrication is established based on Navier–Stokes equations. The FLUENT software is used to simulate and analyze the four texture models, explore the dynamic pressure lubrication characteristics of different texture types, and provide data support for texture optimization. The key variable values required by the mathematical model are obtained through the simulation data. The friction coefficient of the texture under different working conditions was measured through friction and wear experiments, and the mathematical model was verified by the experimental results. The research results show that circular texture is suitable for low to medium speed and high load conditions, chevron texture is suitable for medium to high speed and medium to high load conditions, groove texture is suitable for high speed and low load conditions, and composite texture is suitable for high speed and medium to high load conditions. Comparing the experimental results with the results obtained by the mathematical model, it is found that the two are basically the same in the ranking of the anti-friction performance of different textures, and there is an error of 10%—40% in the friction coefficient value. In this study, a mathematical model of hydrodynamic lubrication was proposed, and the solution method of the optimal surface texture model was determined.

Keywords: Hydrodynamic lubrication, Tribological characteristics, Surface texture

1 Introduction

As an effective means of reducing friction, texture has a very broad industrial application prospect. The working mechanism of texture [1, 2] is the theoretical basis of its optimal design. Many studies usually comprehensively analyze the tribological theory and test results, and continuously improve the design of the texture to make it more adaptable [3, 4].

Wakuda Manabu et al. [5] found that there is a certain size and area ratio to optimize the friction characteristics of the friction pair, while the shape parameters of the texture have little effect on the friction performance. Krupka et al. [6] explored the effect of micro-pit morphology on the thickness of the oil film. The study found that the micro-pit shape can increase the thickness of oil film. Rahmani et al. [7] used an optimization program to find the best dimensional parameters to increase the pressure-bearing capacity and lubricant flow ratio of the asymmetrically textured slider bearing and reduce the friction coefficient. Charitopoulos et al. [8] found that textures of different shapes and sizes show different

*Correspondence: me_yangxf@ujn.edu.cn
[1] College of Mechanical Engineering, University of Jinan, Jinan 250022, China
Full list of author information is available at the end of the article

improvements on the friction resistance of friction surfaces. Andersson et al. [9] found that the texture with low density and large depth-to-diameter ratio combined with high viscosity lubricating oil can increase the anti-friction properties. Yang et al. [10] studied the influence of the cross-sectional shape of the texture on the hydrodynamic lubrication. The results show that under the condition of low load and low speed, the spherical texture with depth-to-width ratio of 0.2 significantly reduces the surface friction coefficient. Wang et al. [11] conducted a fretting wear experiment on the texture of grooves with different orientations, and studied the filling effect of the debris in the grooves with different orientations on the texture. Lu et al. [12] studied the effect of anisotropic texture on friction properties. The results show that the triangular texture has a better drag reduction effect than the rectangular texture. Codrignani et al. [13] used concomitant optimization techniques to determine the topography of the two surfaces in relative motion under thin lubricating film conditions. Tu et al. [14] used the level set method to optimize the shape of the texture to maximize the bearing capacity of the surface under hydrodynamic lubrication conditions. However, this optimization method has the disadvantage of relying too much on the initial texture. Wang et al. [15] used GA-SQP hybrid method to optimize the groove texture. The results show that the chevron textured surface has an ultra-low friction coefficient. Shen et al. [16] studied the effect of chevron texture arrangement on the lubrication performance. The research results show that the chevron texture of the V-shaped arrangement has better lubricating performance than the texture of the rectangular arrangement. Liu et al. [17] found that the pit texture with 28.26% area density has a better drag reduction effect than other textures. Chen et al. [18] found that when the area density of texture is greater than 9%, the bearing capacity of the oil film can be significantly improved. Our group [19] studied the influence of the area density of chevron texture on the tribological properties. The results show that the area density of 10% is beneficial to reduce friction and achieve stable lubrication performance.

Lubricating conditions can affect the anti-friction mechanism of texture [20]. The friction wear test results alone cannot explain the working mechanism of the surface texture under a certain lubrication condition [21, 22]. The lubrication state of the contact surface is closely related to the oil parameters [23]. Thickness of oil film and surface roughness can be used to determine the lubrication state under different operating conditions [24].

Ryk et al. [25] found that the friction force of the laser-processed surface textured cylinder liner piston ring was reduced by 25%. This is because the surface texture enhances the hydrodynamic lubrication effect under high-speed reciprocating motion. Tønder [26] believes that the surface texture can store lubricant in the inlet area. Therefore, the rigidity and damping of the lubricating oil film can be improved, thereby improving the stability of the oil film. Kligerman et al. [27] studied the hydrodynamic effects of laser surface texture in sealed micropores. The results show that, the texture can effectively reduce the friction torque. Suh et al. [28] found that the surface texture reduces the adhesion and friction by reducing the effective contact area between the slider and the medium surface. Chen et al. [29] studied the high-pressure dynamic lubrication properties of textured mechanical sealing pair. The research results show that, compared with the untextured sealing pair, the multi-scale composite textured sealing pair produces a lower and more stable friction torque. Yagi et al. [30] studied the effect of texture on surface lubrication characteristics under starved hydrodynamic lubrication conditions. The research results show that the groove texture can reduce the friction coefficient under high sliding conditions. Galda et al. [31] conducted experiments to study the effect of texture on the performance of the bearing. The study found that the textured bearing surface significantly reduces the coefficient of friction during the shutdown period compared to smooth surface. However, under the condition of stable load and speed, the friction torque of the textured bearing surface is increased by 41% compared with the smooth surface. The results show that the effect of surface texture on the sliding surface is controversial. At present, it is necessary to continue to develop textures to select textures suitable for specific working conditions.

The research of this paper focuses on establishing a mathematical model for the different characteristics of surface textures, which can reflect the tribological characteristics of each texture. In this paper, a mathematical model of hydrodynamic lubrication with different surface textures is established based on the Navier–Stokes equation. Through FLUENT simulation analysis and friction and wear experiments, the friction reduction and dynamic pressure lubrication mechanisms of different surface textures are explored. According to the simulation results, the key variables of the mathematical model are solved, and the mathematical model is verified by the experimental results. Finally, the solution method of the optimal surface texture model is determined, and a set of optimal selection equations for surface texture under different working conditions is summarized. By studying the tribological characteristics of surface textures with different morphology and size characteristics, the optimal surface texture can be solved and manufactured according to the working conditions of the sliding friction pair.

2 Establishment of Mathematical Model

In this paper, based on the Navier–Stokes equation (N–S equation), a mathematical model of hydrodynamic lubrication of different surface textures was established, and the solution method of the optimal surface texture model was determined. The purpose is to study how to choose the optimal solution for different surface textures under different working conditions, and provide theoretical guidance for subsequent research.

2.1 Introduction to Basic Theory

2.1.1 Derivation of N–S Equation

The N–S equation is obtained by substituting and sorting the components of the viscous fluid motion momentum equation in the form of stress with the expression given by the generalized Newton's internal friction law. If the fluid is incompressible, the dynamic viscosity μ is constant. The N–S equation can be simplified as:

$$\begin{aligned}\rho\frac{\mathrm{d}v_x}{\mathrm{d}t} &= \rho f_x - \frac{\partial p}{\partial x} + 2\mu\frac{\partial^2 v_x}{\partial x^2} + \mu\frac{\partial}{\partial y}\left(\frac{\partial v_x}{\partial x} + \frac{\partial v_x}{\partial y}\right)\\ &\quad + \mu\frac{\partial}{\partial z}\left(\frac{\partial v_x}{\partial z} + \frac{\partial v_z}{\partial x}\right) = \rho f_x - \frac{\partial p}{\partial y} + \mu\nabla^2 v_x\\ \nabla^2 &= \frac{\partial^2}{\partial x^2} + \frac{\partial^2}{\partial y^2} + \frac{\partial^2}{\partial z^2}.\end{aligned} \tag{1}$$

Similarly, equations in the form of projections on the y and z axes can be derived. The two ends of the equation are divided by the density at the same time, and the three projection forms of the N–S equation of incompressible viscous flow can be obtained from the relationship of dynamic viscosity μ, kinematic viscosity and density.

$$\begin{aligned}\frac{\mathrm{d}v_x}{\mathrm{d}t} &= f_x - \frac{1}{\rho}\frac{\partial p}{\partial x} + \nu\nabla^2 v_x,\\ \frac{\mathrm{d}v_y}{\mathrm{d}t} &= f_y - \frac{1}{\rho}\frac{\partial p}{\partial y} + \nu\nabla^2 v_y,\\ \frac{\mathrm{d}v_z}{\mathrm{d}t} &= f_z - \frac{1}{\rho}\frac{\partial p}{\partial z} + \nu\nabla^2 v_z.\end{aligned} \tag{2}$$

2.1.2 Couette Flow

The N–S equation of viscous fluid motion is a second-order nonlinear partial differential equation, which is difficult to be solved. In addition, in practical engineering, the viscous flow with complex flow boundaries is encountered, and with the change of time and space, the flow parameters in the flow field are also constantly affected and changed. But when the flow boundary is relatively simple and the flow parameters are mostly constant, the solution of the flow can be obtained. As a kind of viscous flow, Couette flow is of great significance in engineering, and accurate analytical solutions can be obtained under some conditions [32].

The typical form of Couette flow is two infinite planes with a distance of h_0, in which an incompressible fluid with a dynamic viscosity of μ flows in a fixed direction. Couette flow also includes two other forms. The first is that there is a speed difference between the two planes, so that the two planes produce relative motion but the pressure in the direction of flow does not change. The second is that there is not only a speed difference between the two planes, but also a pressure gradient in the flow direction. At this time, the solution of the linear equation is additive, and the independent solutions of velocity and pressure can be added.

2.2 Basic Derivation of Theory

Each surface texture corresponds to one or more pressure values and velocity values that can give full play to its tribological properties. This matching mechanism is the core of theory.

Before deriving the basic theory, the applicable premise must be determined first:

1. The effects of volume force such as gravity and magnetic force are ignored.
2. Assume that there is no relative sliding between the fluid and solid interface.
3. The fluid belongs to a kind of Couette flow, but it is not exactly the same.
4. The fluid is Newtonian fluid, and the flow mode is turbulent flow. There may be vortex and turbulent flow in the oil film.
5. Compared with the viscous force of lubricating oil, the inertial force is smaller, so its effect is ignored, including the inertial force when the fluid accelerates and the centrifugal force when the fluid moves in a circular motion.

2.2.1 Setting of Fluid Boundary Conditions Based on Couette Flow

As shown in Figure 1, the thickness of the oil film between the two moving friction pairs is h_0. The lubricating oil is an incompressible fluid with a dynamic viscosity of μ, which is driven by the upper plate to flow positively towards the X axis, and the moving speed of the upper plate is U. The depth of texture is h_p, and the cross-sectional width is $2r_\mathrm{p}$. The upper plate moves to the right at speed U, while the lubricating oil has a pressure gradient in the x direction. The red line represents the speed gradient change. The purple line represents the velocity distribution under different pressures. When $P>0$, the velocity distribution is the rightmost purple line,

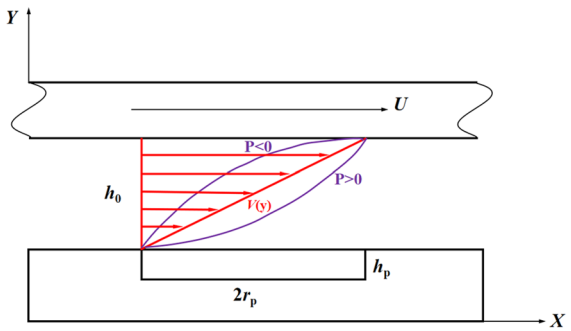

Figure 1 Couette flow

the pressure promotes the flow of lubricating oil, and the average velocity is greater than the velocity without pressure difference. When $P<0$, the velocity distribution is the leftmost purple line. At this time, the flow caused by the upper plate is not enough to overcome the flow caused by the reverse pressure difference, so reverse flow occurs.

The N–S equation can be reduced to:

$$v_x(y) = U\frac{y}{h_0} - \frac{1}{2\mu}\frac{\mathrm{d}p}{\mathrm{d}x}y(h_0 - y). \tag{3}$$

By dividing both sides of Eq. (3) by y, the equation becomes:

$$\frac{v_x(y)}{y} = U\frac{1}{h_0} - \frac{1}{2\mu}\frac{\mathrm{d}p}{\mathrm{d}x}(h_0 - y). \tag{4}$$

Eq. (4) is the relationship between the fluid velocity and pressure in the Couette flow form. This equation is a simplified N–S equation based on Couette flow.

2.2.2 Summary of Theory Formula

Substituting Eq. (4) into the pressure-friction conversion equation (Eq. (5)), Eq. (6) is obtained.

$$f = \frac{\frac{\mathrm{d}p}{\mathrm{d}x\cdot(D_1+D_2)}(D_1^2 - D_2^2)\pi}{n} = \frac{\frac{\mathrm{d}p}{\mathrm{d}x}}{n}(D_1 - D_2)\pi, \tag{5}$$

$$f = \frac{\frac{U}{h_0} - \frac{v_x(y)}{y}}{(h_0 - y)} \cdot \frac{2\mu}{n} \cdot (D_1 - D_2)\pi. \tag{6}$$

The conversion Eq. (5) is derived from the actual experimental conditions in this paper. $\mathrm{d}p/\mathrm{d}x\cdot(D_1-D_2)/n$ is the pressure value in the unit area, n is the number of texture distribution on the surface of the test piece, D_1 is the inner diameter of the grinding piece, D_2 is the outer diameter of the grinding piece. Eq. (5) can be used to combine the hydrodynamic equations with the surface texture parameters, and fully fit the actual working conditions of this article, which improves the accuracy and credibility of the equation. However, there is a certain error in the solution of the pressure in the cell texture area, and this equation also has a certain error. Eq. (6) is the relationship between friction force and fluid flow characteristics, it is necessary to continue to derive the equation. The final Eq. (7) is obtained.

$$\frac{F}{f} = \frac{P\cdot S}{f} = \frac{P\cdot S(h_0 - y)\cdot n}{(\frac{U}{h_0} - \frac{v_x(y)}{y})\cdot 2\mu(D_1 - D_2)\pi}. \tag{7}$$

2.3 Simplification of Theory Formula

According to the experimental conditions in this paper, the substitution amount is simplified. The outer diameter, inner diameter and contact area of the grinding piece are fixed. The lubricating oil is selected from Mobil Series No. 1 lubricating oil, and the parameters are fixed. In Eq. (7), the value of h_0 is critical. Since there is an independent variable y in the film thickness direction, if h_0 is retained, it will increase the difficulty of solving and make the equation have multiple solutions. The value of h_0 is set to 1, and the range of the independent variable y is [0, 1], and Eq. (8) is obtained.

$$\begin{aligned} u &= \frac{P\cdot 0.0000885\cdot(1-y)\cdot 24}{(\frac{U}{1} - \frac{v_x(y)}{y})\times 2\times 0.055\times(0.01+0.014)\pi} \\ &= \frac{P\cdot(1-y)\cdot 0.002124}{0.0083\cdot(\frac{U}{1} - \frac{v_x(y)}{y})}. \end{aligned} \tag{8}$$

In Eq. (8), the pressure P and speed U need to be set according to the actual working conditions. In this model, the velocity v at any point has only the x-axis component, $v_y=v_z=0$, so it can be considered that $v_x=v$. This part needs to obtain data through simulation to solve, the solution process is explained in detail in the simulation analysis section.

3 Simulation Analysis

The FLUENT module in ANSYS software was used to simulate the hydrodynamic lubrication effect. The purpose is to obtain data that cannot be obtained under experimental conditions to provide data support for the model solution.

3.1 Process of Simulation Analysis

In this paper, four kinds of surface textures are selected as the research object, including groove texture, composite texture, chevron texture and circular texture. The groove texture and the circular texture are typical

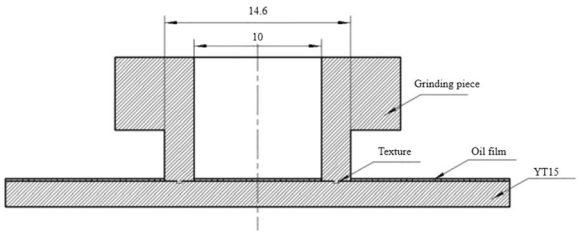

Figure 2 Schematic diagram of experiment

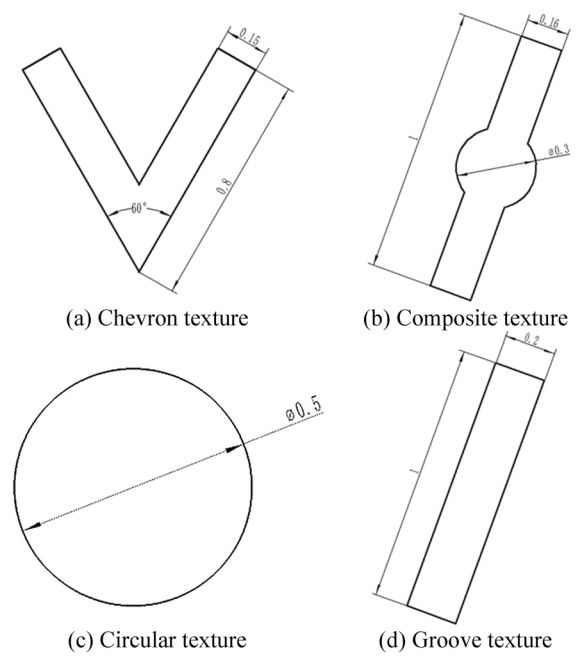

(a) Chevron texture (b) Composite texture

(c) Circular texture (d) Groove texture

Figure 3 The size of the texture

textures. As new types of texture, chevron texture and composite texture have great research value. The upper sample is 45 steel with an inner diameter of 10 mm and an outer diameter of 14.6 mm, and the lower sample is a round YT15 cemented carbide, as shown in Figure 2. The texture size is shown in Figure 3.

If the thickness of the oil film is too large, it is inconsistent with the reality, and if it is too small, the hydrodynamic lubrication effect cannot be reflected. The thickness of the oil film was set to half of the texture depth. The meshing adopted a mixed mesh of unstructured tetrahedron and hexahedron. Encryption processing was performed at the boundary of the surface and near the texture. ICEM CFD was used for meshing. The fluid in the simulation model is lubricating oil. Viscosity grade is ISO VG 68, density is 895 kg/m^3, viscosity is 61.8×10^{-6} mm^2/s. The model selected the k-ε turbulence model and used Enhanced Wall Treatment. The upper end face was set as the pressure input face. The inner and outer rings of the model were set as pressure output surfaces. In actual experiments, the pressure on both sides is atmospheric pressure. Therefore, the output surface pressure value in the simulation model is zero. The other surface was set as a moving wall and rotates around the center according to the rotation speed. The pressure value was calculated according to the loading force values in the actual experiment −50 N, 100 N, 150 N and 200 N. The pressure value was obtained from Eq. (9):

$$P = \frac{F}{S} = \frac{50\ \text{N}}{0.0000887\ \text{m}^2} = 562429.7\ \text{Pa}. \tag{9}$$

The input pressure is 562429.7 Pa at a load of 50 N, and was set to 560000 Pa during simulation. Similarly, the pressure value is 1120000 Pa at a load of 100 N, is 1680000 Pa at a load of 150 N, and is 2240000 Pa at a load of 200 N. The empirical value of the turbulence intensity was 10%, and the hydraulic diameter was calculated by Eq. (10):

$$D = \frac{4A}{P} = \frac{4 \times 1 \times 0.15\ \text{mm}^2}{2.3\ \text{mm}} = 0.26\ \text{mm}. \tag{10}$$

Where A is the cross-sectional area of the model and P is the cross-sectional circumference of the model.

The upper end face was set as the speed inlet. The speed value was based on the speed value in the actual experiment −50 r/min, 100 r/min, 120 r/min, 150 r/min, 180 r/min and 200 r/min. It can be calculated by Eq. (11):

$$v = \frac{r}{T} = \frac{0.006 \times 100\ \text{m/s}}{60} = 0.01\ \text{m/s}. \tag{11}$$

When the rotation speed is 100 r/min, the average linear velocity of the grinding piece is 0.01 m/s. Similarly, when the rotation speeds are 50 r/min, 120 r/min, 150 r/min, 180 r/min and 200 r/min, the corresponding linear velocity values of simulation model are 0.05 m/s, 0.12 m/s, 0.15 m/s, 0.18 m/s and 0.2 m/s. The algorithm used the SIMPLE method. The momentum equation adopted two-level upwind style discreteness. The remaining energy equations adopted the first-order upwind style discreteness. The relaxation factors remained at their default values. The calculation starting point was the input face.

3.2 Simulation Results

Figure 4 shows the total pressure cloud diagram and dynamic pressure cloud diagram of the four textures under the same experimental conditions (50 N, 100 r/min). As shown in Figure 4(a), the high-pressure areas of

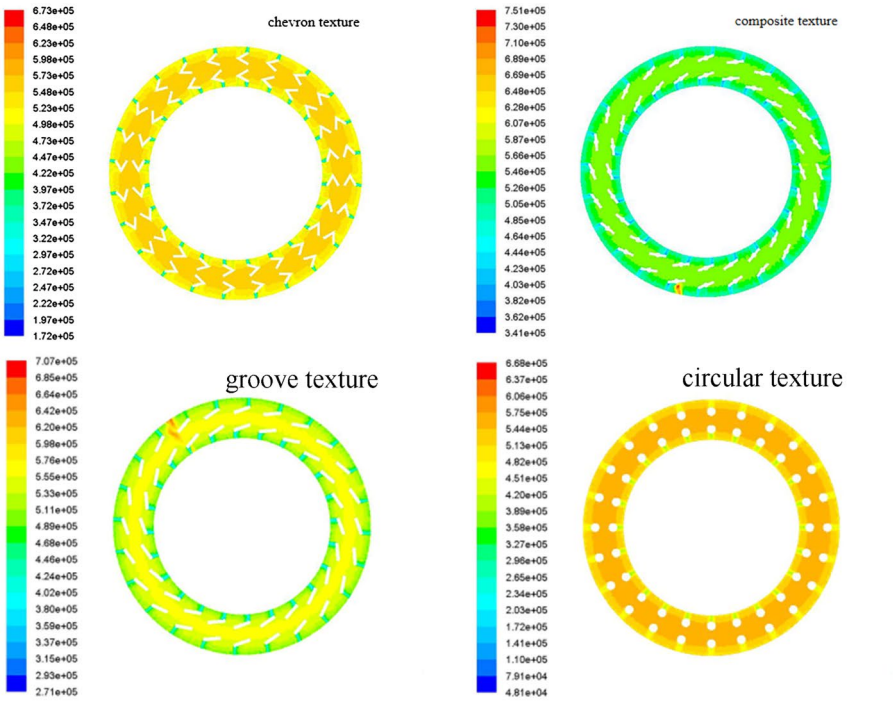

Figure 4 Overall pressure cloud diagram and dynamic pressure cloud diagram of overall texture

the four textures are in the middle of the double-row texture. The high-pressure areas of chevron, composite, and circular textures are more concentrated and the boundaries are obvious, while the high-pressure areas of the groove texture have blurred boundaries, and there is no significant difference in pressure values across the texture surface. From the numerical point of view, the pressure value of the circular texture is the largest, the pressure value of the chevron texture is second only to the circular texture, and the pressure value of the groove texture is the smallest. As shown in Figure 4(b), the dynamic pressure distribution on the surface of the four textures is basically the same, and they are relatively small. This is because the dynamic pressure value at the position close to the wall is smaller than the center position of the fluid flow.

3.3 Numericalization of Simulation Results

3.3.1 Data Collection

When constructing a mathematical model, the partial derivative of velocity v with respect to y is unknown. Because it is not easy to measure in actual experiments, it needs to be calculated according to the simulation analysis results. Using FLUENT software, the velocity clouds of the four textures are obtained when the loading force is 50 N and the rotation speed is 100 r/min. The results are shown in Figure 5. According to the simulation results, a vertical line is taken at the output end face, as shown in Figure 6. FLUENT's data processing function is used to output ASCII code data, and then Notepad ++ is used to import the data into an Excel table after processing. The values in the data include x-coordinate, y-coordinate, z-coordinate, and velocity-magnitude. According to the theoretical analysis part, the value of $v_x(y)$ is velocity-magnitude. And according to Figure 6, the speed value is 100−300 mm/s, the actual speed is about 1−10 mm/s, so in order to rigorous and accurate mathematical model, the data needs to be processed. All simulation values were reduced by 100 times.

3.3.2 Simulation Equations of Key Variables

After obtaining the simulation data value, the function equation is solved according to the numerical value, and the solving process is carried out with the help of MATLAB toolbox. The processed data was imported into the MATLAB workspace and named for different data groups. The Curve Fitting toolbox was selected to perform curve fit analysis on the data in the work area to obtain a function equation. Figure 7 shows the fitting curves of four textures. The abscissa is the y value, and the y-axis zero position is at the top of the data selection line in Figure 6. The ordinate is the speed value. R-square is the degree of equation fit. To facilitate the solution of the mathematical model, replace y in the original formula with x. The four texture fitting equations are shown in Table 1.

4 Friction and Wear Experiment

4.1 Design of the Experiment

4.1.1 Design of Surface Texture

The area occupancy rate of the four textures is 10%. The processing parameters of the four textures are shown in Table 2.

Before processing the texture on the surface of the workpiece, it is necessary to pre-treat the test piece. Boron carbide powder was used to grind the test piece to smooth on frosted glass. Diamond polishing paste was used to polish the test piece on the polishing machine until the surface was mirror-like. The test piece was placed in an ultrasonic cleaner to clean the surface dirt. The polished samples were measured on a Mitutoyo SJ-410 surface roughness measuring instrument and the average surface roughness of all test pieces was 0.045. A Libra-HE femtosecond laser was used to process the surface texture.

4.1.2 Experimental Scheme

The experiment used MMG-10 friction and wear testing machine. The lubricating oil code is 5W-40, and the viscosity at normal temperature is 0.055 Pa·s. The variable selects the loading force and speed, and the parameter values are shown in Table 3. Four variables were selected for the loading force and six variables for the rotation speed, and a total of 96 groups of experiments were conducted, each group of experiments for 10 min. Figure 8 shows the MMG-10 friction and wear testing machine, 45 steel, and textured specimens used in the test.

4.2 Experimental Results

4.2.1 Chevron Texture

Figure 9 is the experimental results of chevron texture under different loading force and speed. According to the three-dimensional graph, the distribution interval of the friction coefficient of chevron texture is [0.05, 0.14], and the range is 0.09. The lowest point of the entire curved surface is when the loading force is 150 N and the rotation speed is 120 r/min. The highest points are at the loading force of 200 N and the speed of 50 r/min and the loading force of 50 N and the speed of 200 r/min, respectively. The point where the friction coefficient is the smallest is the value when the loading force and the rotation speed are at an intermediate level. The friction coefficient at a loading force of 50 N and a rotation speed of 50 r/min and a loading force of 200 N and a rotation speed of 200 r/min are close and small. This shows that there is an optimal matching interval between loading

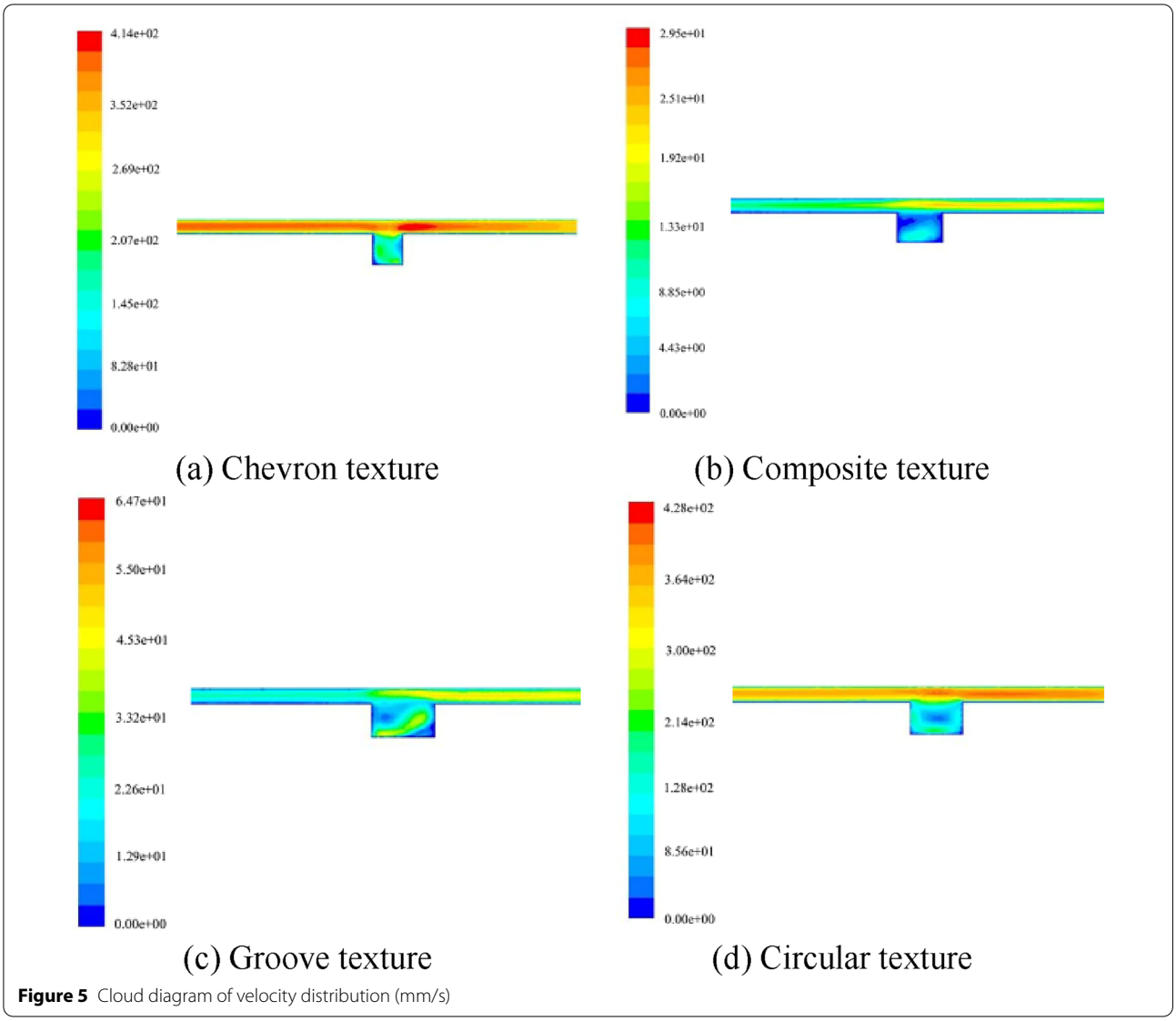

Figure 5 Cloud diagram of velocity distribution (mm/s)

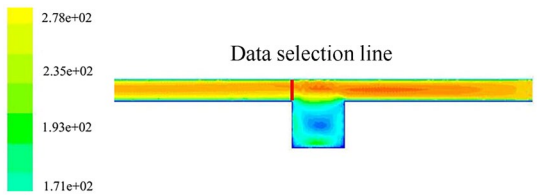

Figure 6 Schematic diagram of the location of the data selection line (mm/s)

force and speed. When the difference between loading force and speed is too large, the friction coefficient will increase. When the speed is constant, the friction coefficient decreases with increasing loading force. When the loading force is constant, the friction coefficient decreases with increasing speed. When the loading force is 200 N, the friction coefficient is small and the change is relatively stable, indicating that the chevron texture shows good hydrodynamic lubrication characteristics under high load conditions. It proves that the chevron texture has strong pressure bearing capacity and is suitable for high load conditions.

4.2.2 Composite Texture

According to the three-dimensional diagram of Figure 10, the distribution interval of the friction coefficient of the composite texture is [0.03, 0.148], and the range is 0.118. The entire curved surface presents a two-step shape. The lowest point of the curved surface is when the loading force is 50 N and the rotation speed is 150 r/min, and the

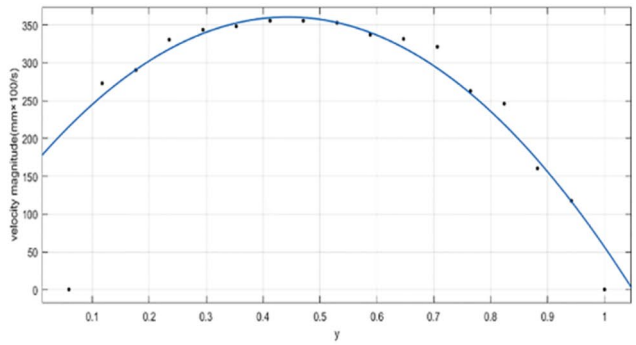

(a) chevron texture

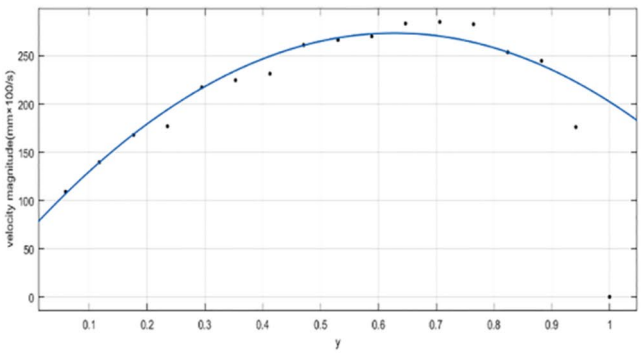

(b) composite texture

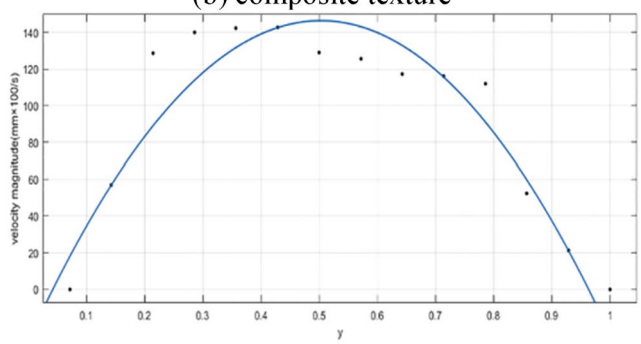

(c) groove texture

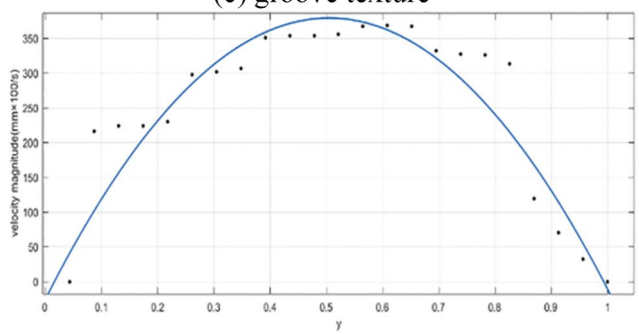

(d) circular texture

Figure 7 Fitting curves of four textures

Table 1 Simulation equations of four textures

Texture	Chevron texture	Composite texture	Groove texture	Circular texture
Equation	$f(x) = P_1 \cdot x^2 + P_2 \cdot x + P_3$	$f(x) = P_1 \cdot x^2 + P_2 \cdot x + P_3$	$f(x) = P_1 \cdot x^2 + P_2 \cdot x + P_3$	$f(x) = P_1 \cdot x^2 + P_2 \cdot x + P_3$
P_1	− 9.52	− 5.146	− 6.904	− 15.90
P_2	8.377	6.462	6.942	16.06
P_3	1.791	0.7071	− 0.2811	− 0.2623
R-square	0.946	0.912	0.8769	0.8741

Table 2 Processing parameters of four textures

Texture	Chevron texture	Composite texture	Groove texture	Circular texture
Distribution form	Double row	Double row	Double row	Double row
Unit number	48	48	48	48
Area of unit texture (mm^2)	0.2	0.19	0.2	0.2
Area occupancy rate (%)	10.8	10	10.8	10.8

Table 3 Experimental parameter values

Texture	Loading force (N)	Rotation speed (r/min)	Condition	Contact method
Chevron texture Composite texture Groove texture Circular texture	50 100 150 200	50 100 120 150 180 200	25 ℃ Atmospheric pressure Oil lubrication	Face to face

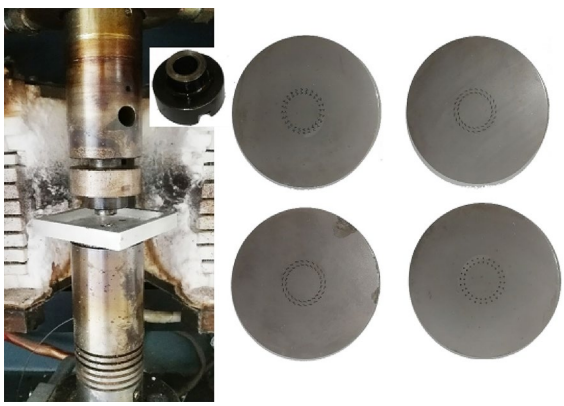

Figure 8 Friction and wear testing machine, 45 steel, and test piece after processing texture

loading force is 50 N and the rotation speed is 200 r/min. The highest points are when the loading force is 50 N and the rotation speed is 50 r/min, and the loading force is

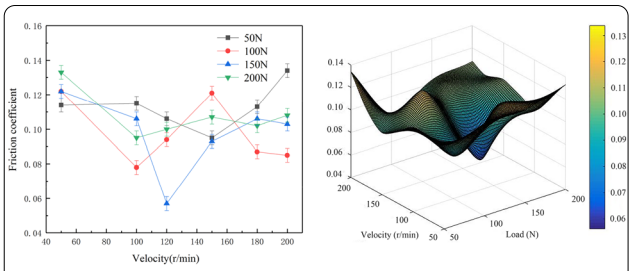

Figure 9 Experimental results of chevron texture

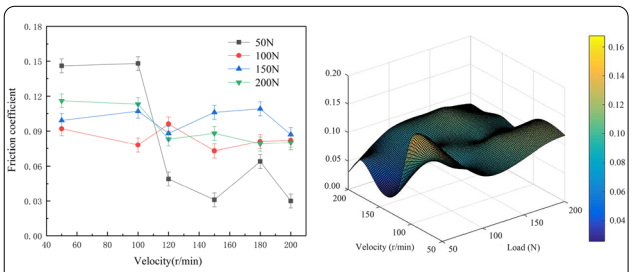

Figure 10 Experimental results of composite texture

50 N and the rotation speed is 100 r/min. Both the maximum and minimum friction coefficients are when the loading force is 50 N. When the rotation speed is greater than 100 r/min, the friction coefficient will appear a stepwise decline under each loading force, and then it will tend to be gentle. When the loading force is 50 N, the range of friction coefficient is extremely large, and the fluctuation is severe. At low speeds, the friction coefficient increases with increasing loading force. At high speeds, the friction coefficient decreases with decreasing

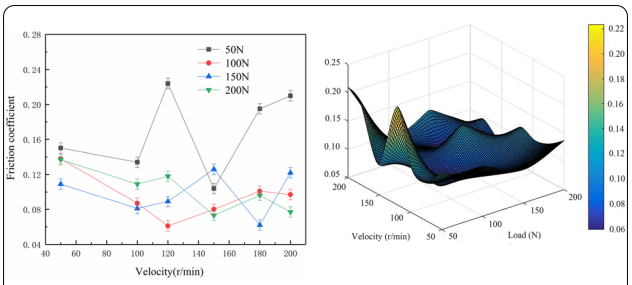

Figure 11 Experimental results of groove texture

loading force. This shows that for composite textures, the influence of speed is greater than the loading force. As shown in the line chart, when the rotation speed is constant, the friction coefficient fluctuates with the increase of the loading force. When the loading force is constant, the friction coefficient decreases with increasing speed. When the loading force is 100 N or above, the friction coefficient value is small and tends to be stable. When the loading force is 100 N, the friction coefficient is more stable and smaller than when the loading force is 150 N and 200 N. It shows that the composite texture shows good hydrodynamic lubrication characteristics under high-speed and medium-high load conditions. It is proved that the composite texture contains the characteristics of groove texture and circular texture, and has a certain pressure-bearing capacity and the ability to promote the flow of lubricating oil.

4.2.3 Groove Texture

According to the three-dimensional graph of Figure 11, the distribution interval of the groove-type texture friction coefficient is [0.061, 0.224], and the range is 0.163. The overall figure presents a double hump-like parallel distribution. The highest point is when the loading force is 50 N and the speed is 120 r/min. The lowest points are when the loading force is 100 N and the rotation speed is 120 r/min, and the loading force is 150 N and the rotation speed is 180 r/min. When the loading force is 50 N, the friction coefficient fluctuates violently and the range is large. When the loading force is 200 N, the surface changes smoothly and the friction coefficient is stable. When the loading force is constant, the friction coefficient is distributed in a hump shape as the speed increases. When the speed is constant, the friction coefficient is distributed in a hump shape as the loading force increases. As shown in the line chart, there is no obvious stepwise decline and level change in the friction coefficient when the loading force is 100 N, 150 N and 200 N. When the rotation speed is between 100 and 150 r/min, each loading force has a small friction coefficient. It shows that the groove texture shows good anti-friction characteristics under medium speed conditions. It is proved that the groove texture has weak pressure bearing capacity and is suitable for medium speed and low load conditions.

4.2.4 Circular Texture

According to the three-dimensional diagram of Figure 12, the distribution interval of the circular texture friction coefficient is [0.045, 0.198], and the range is 0.153. The highest point is when the loading force is 50 N and the speed is 100 r/min. The lowest points are when the loading force is 100 N and the rotation speed is 100 r/min, and the loading force is 50 N and the rotation speed is 200 r/min. The friction coefficient fluctuates greatly when the loading force is 50 N, and the curved surface is hump-shaped. The friction coefficient gradually stabilizes with the increase of the loading force, and it shows a plane-like distribution. As shown in the line chart, when the speed is constant, the friction coefficient decreases with the increase of the loading force. When the loading force is 200 N, the friction coefficient is small and the change is relatively stable. When the loading force is constant, the friction coefficient increases with the increase of speed. When the rotation speed is 100 r/min and the loading force is 100 N, 150 N, and 200 N, the friction coefficient is the minimum value under the loading force. It shows that the circular texture shows excellent stability under high load and medium speed conditions. It is proved that the circular texture has strong pressure bearing capacity and strong stability, and is suitable for high load conditions.

4.2.5 Friction Coefficients of Different Textures under the Same Loading Force

Figure 13 is the variation curve of friction coefficient of different textures under the same loading force. When the loading force is 50 N, 100 N and the rotation speed is low, the friction coefficient of chevron texture and circular texture is the lowest. At high speeds, the friction reduction effect of the composite texture is most obvious. When the loading force is 150 N, the friction coefficient of chevron, composite and circular texture changes in the same trend, showing a large undulating wave shape. The rotation speed at the lowest friction coefficient of the circular texture is 100 r/min, the chevron texture is 120 r/min, and the groove texture is 180 r/min. The friction coefficient of the composite texture changes steadily and there are no huge fluctuations. When the loading force is 200 N and the rotation speed is low, the friction coefficient of chevron texture and circular texture is lower. At

high speeds, the friction coefficient of the composite texture and the groove texture is lower. The chevron texture has a strong pressure-bearing ability, but it can only play a good anti-friction effect at low speeds, and the anti-friction effect decreases significantly at high speeds. Due to the weak pressure bearing capacity of the groove texture, the friction coefficient is unstable under high load. However, due to the characteristics of improving fluidity, the friction coefficient is small at high speeds. The composite texture consists of groove and circle. The composite texture still shows good anti-friction effect under high load and high speed working conditions.

The above research shows that the chevron texture has a small and stable friction coefficient at high loads. It shows that chevron texture is suitable for high load conditions. The composite texture has a small friction coefficient under high-speed and medium-high load conditions. It shows that the composite texture is suitable for high-speed and medium-high load conditions. The friction coefficient of the groove texture does not decrease significantly when the loading force increases. When the rotation speed is constant, the friction coefficient decreases as the loading force decreases. It shows that the pressure capacity of the groove texture is weak, and it is suitable for medium speed and low load working conditions. The friction coefficient of the circular texture tends to be stable as the loading force increases. When the loading force is constant, the friction coefficient will increase with the increase of speed. It shows that the circular texture has strong pressure bearing capacity and weak flow promotion ability, which is suitable for medium and low speed and high load working conditions.

5 Solution and Verification of Mathematical Model

5.1 Combination of Simulation Formula and Theoretical Formula

5.1.1 Determination of Key Parameters

According to the simulation model, the oil flow velocity equations under different surface texture conditions are obtained, and the first derivative is obtained by combining the mathematical model with the results. The results are shown in Table 4. After obtaining the key equation, it is substituted into the theory equation.

5.1.2 Substitution of Key Parameters

The above key equation is substituted into Eq. (8) to obtain Eq. (12):

$$u = \frac{P \cdot (1-x) \cdot 0.002124}{0.0083 \cdot (U - F'(x))}. \tag{12}$$

Eq. (12) is further simplified to obtain Eq. (13):

$$u = \frac{0.256 \cdot P(1-x)}{(U - 2 \cdot K_1 \cdot x - K_2)}. \tag{13}$$

Where K_1 and K_2 are equation parameter values of different surface textures. The equations of the four surface textures are as follows.

The equation of chevron texture is:

$$u = \frac{0.256 \cdot P(1-x)}{(U + 19.04 \cdot x - 8.377)}. \tag{14}$$

The equation of composite texture is:

$$u = \frac{0.256 \cdot P(1-x)}{(U + 10.292 \cdot x - 6.462)}. \tag{15}$$

The equation of groove texture is:

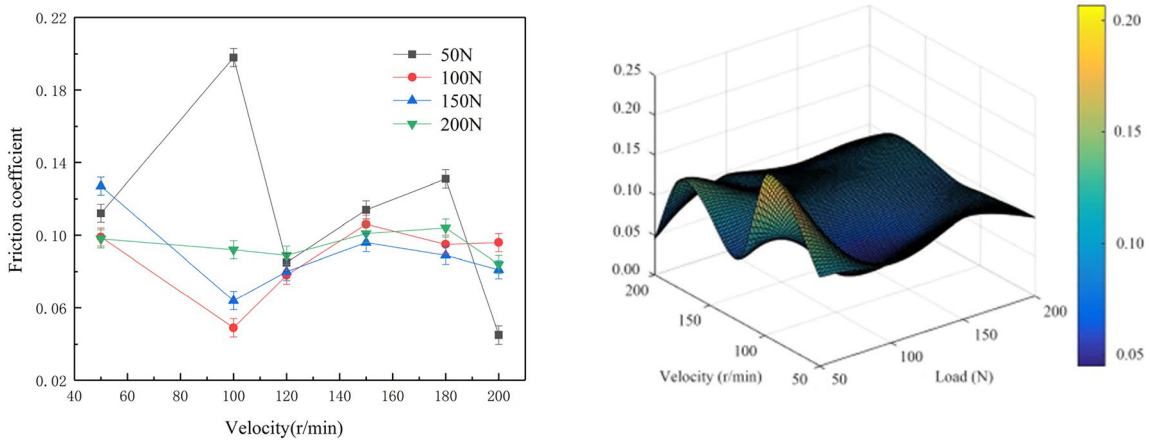

Figure 12 Experimental results of circular texture

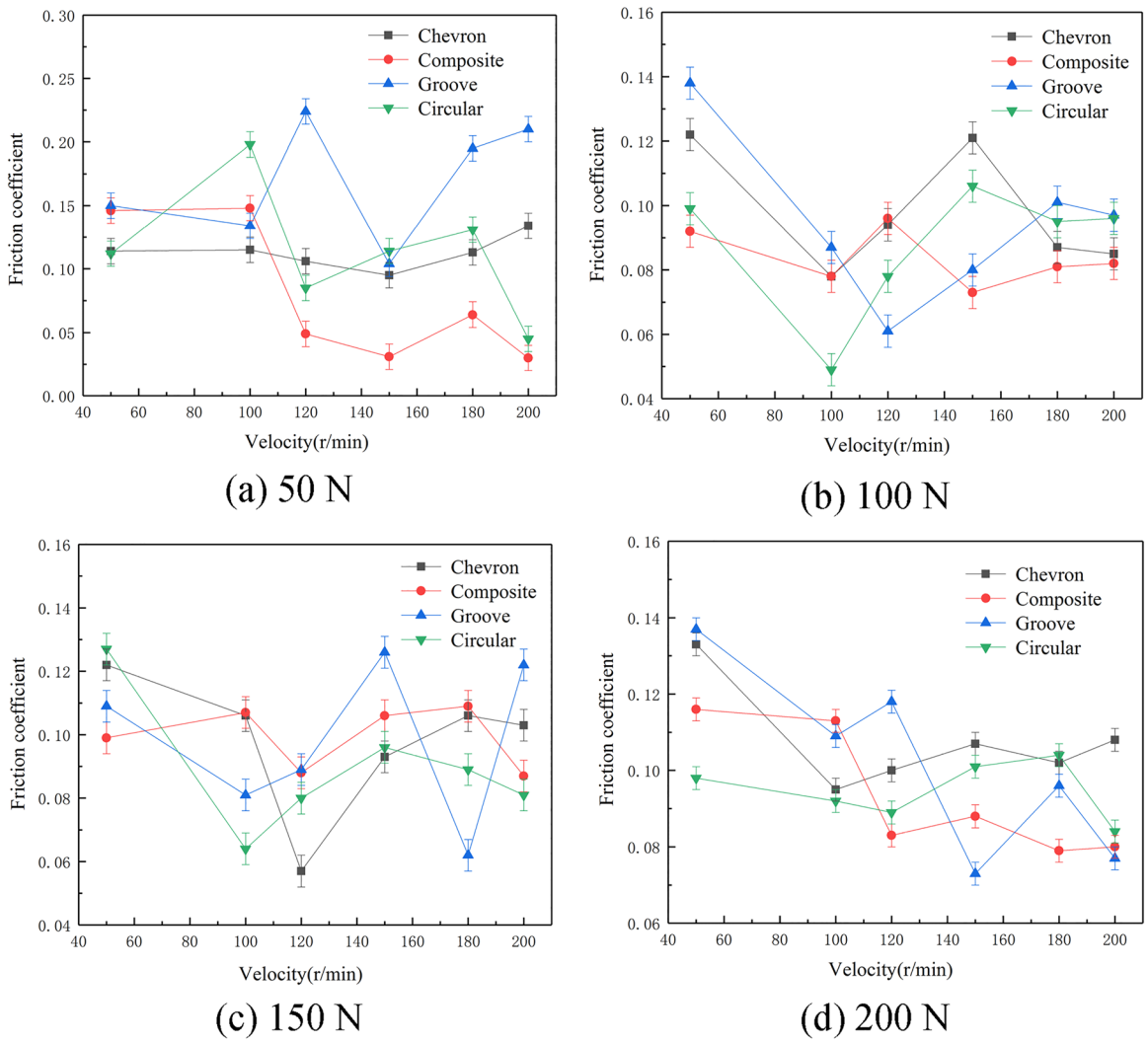

Figure 13 Variation curve of friction coefficient of different textures under the same loading force

$$u = \frac{0.256 \cdot P(1-x)}{(U + 13.808 \cdot x - 6.942)}. \tag{16}$$

The equation of circular texture is:

$$u = \frac{0.256 \cdot P(1-x)}{(U + 31.80 \cdot x - 16.06)}. \tag{17}$$

5.2 Verification of Formula

According to the above equation, the relationship between the friction coefficient u, the load P, and the rotation speed U can be obtained, and the value range of x is [0, 1]. After substituting the loading force and speed under different working conditions into Eqs. (14), (15), (16), and (17), the minimum value of the equation in the interval [0,1] is solved, and the function values of the four equations are compared. The texture with a smaller function value is the better texture, which can achieve the purpose of selecting the optimal texture according to different working conditions.

In order to verify the accuracy of the formula, an experimental working condition was selected to compare the experimental results with the calculation results of the formula. The loading force of 50 N and the speed of 100 r/min are selected to solve the minimum value of the equation. MATLAB software is used to solve the other program. When substituting into the equation, P needs to adopt a unified international unit system, P=560000 Pa. The calculation results and experimental results are shown in Table 5.

According to the calculation results, the order of anti-friction performance of different textures from good to

Table 4 Derivatives of four texture equations

Texture	Chevron texture	Composite texture	Groove texture	Circular texture
Equation	$F'(x) = 2 \cdot K_1 \cdot x + K_2$	$F'(x) = 2 \cdot K_1 \cdot x + K_2$	$F'(x) = 2 \cdot K_1 \cdot x + K_2$	$F'(x) = 2 \cdot K_1 \cdot x + K_2$
K_1	− 9.52	− 6.904	− 6.904	− 15.90
K_2	8.377	6.942	6.942	16.06

bad is as follows: circular, chevron, groove, composite. According to the experimental results, the order of anti-friction performance of different textures from good to bad is as follows: chevron, groove, composite, circular. In terms of friction coefficient, there is a 10%−40% error between the theoretical analysis results and the experimental results. From the simulation analysis, it can be seen that the circular texture is suitable for medium and low speed and high load conditions, and 50 N, 100 r/min are medium speed and low load conditions. The simulation results are consistent with MATLAB calculation results. An important factor that may cause large differences in experimental results may be experimental errors. According to the friction and wear test results of circular texture, the friction coefficient is large under this condition, indicating that there is a greater possibility of errors. Other working conditions were followed the above steps to verify the hydrodynamic lubrication theory. The results prove that the theory has a certain accuracy, but it still has some differences from the actual experimental results, and in-depth research is still needed.

6 Conclusions

(1) In terms of theoretical analysis, this paper uses the Navier-Stokes equation as the theoretical basis, sets Couette flow as the boundary conditions of the model, and combines experimental conditions to establish a mathematical model of hydrodynamic lubrication. The key variables related to speed in the model are unknown and difficult to measure in experiments. Therefore, the variable value is obtained through simulation.

(2) In terms of simulation analysis, this paper uses FLUENT to simulate the hydrodynamic lubrication effect of chevron, composite, groove and circular texture. The results show that chevron texture has strong pressure bearing capacity. The composite texture can bear a certain intensity of load while ensuring the fluidity of the lubricant. The groove texture can effectively increase the flow speed, but the pressure bearing capacity is weak. The average dynamic pressure value of the circular texture is the largest.

Table 5 Calculation results of MATLAB

Texture	Calculation results	Experimental results
Chevron texture	0.0856	0.115
Composite texture	0.0913	0.148
Groove texture	0.0887	0.134
Circular texture	0.0819	0.198

(3) In terms of experimental research, femtosecond laser processing technology is used to process texture on the surface of the workpiece for friction and wear experiments. The test results show that the friction coefficient of chevron texture is small and stable under high load. The friction coefficient of composite texture decreases with the increase of speed, and the coefficient is small and stable when the loading force is 100 N, 150 N. The friction coefficient of groove texture changes little with the increase of loading force, while the coefficient decreases when the rotation speed increases. The friction coefficient of circular texture is the smallest at low to medium speed and medium to high load.

(4) In terms of solving the mathematical model, the key variables obtained from the simulation analysis are substituted into the mathematical model established by the theoretical analysis. After comparing the experimental results with the results obtained by the mathematical model, it is found that the two are basically the same in the ranking of the anti-friction properties of different textures, and there is an error of 10%−40% in the friction coefficient value.

Acknowledgements
Not applicable.

Authors' Contributions
XY was in charge of the whole trial; DL wrote the manuscript; YW, JC, SW, ZW, WL and GX assisted with sampling and laboratory analyses. All authors read and approved the final manuscript.

Authors' Information
Dan Li, is currently a PhD candidate at *University of Science and Technology of China*. She received her master's degree in mechanical engineering from *University of Jinan, China*, in 2021.
Yang Xuefeng, is currently a professor of U*niversity of Jinan*, China.
Yuanbo Wu received his master's degree in mechanical engineering from *University of Jinan, China*, in 2019.
Jian Cheng is currently a professor of *Hubei University of Technology, China.*
Shouren Wang is currently a professor of *University of Jinan, China.*
Zhuang Wan, Wenbo Liu and Guofeng Xia received their master's degree in mechanical engineering from *University of Jinan, China*, in 2021.

Funding
Supported by National Natural Science Foundation of China (Grant Nos. 51575234, 51872122), Postdoctoral Science Foundation of China (Grant No. 2017M620286), Key Research and Development Program of Shandong, Province, China (Grant No. 2018CXGC0809), Major basic research projects of Shandong Natural Science Foundation (Grant No. ZR2020ZD06), Project of Shandong Province Higher, Educational Youth Innovation Science and Technology, Program (Grant No. 2019KJB021), Experts from Taishan Scholars, and Youth Innovation in Science & Technology Support Plan of Shandong Province University.

Availability of data and materials
The datasets used and/or analysed during the current study are available from the corresponding author on reasonable request.

Competing Interests
The authors declare no competing financial interests.

Author Details
[1]College of Mechanical Engineering, University of Jinan, Jinan 250022, China. [2]College of Mechanical Engineering, Hubei University of Technology, Hubei 430068, China. [3]University of Science and Technology of China, Hefei, China.

Received: 16 September 2020 Revised: 4 January 2022 Accepted: 18 February 2022
Published online: 05 April 2022

References

[1] Y Q Xing, J X Deng, Z Wu, et al. High friction and low wear properties of laser–textured ceramic surface under dry friction. *Optics and Laser Technology*, 2017, 93: 24–32.
[2] T Ye, J W Ma, Z Y Jia. Influence of design parameters on the low temperature tribological performance of surface textured aluminium alloy. *Journal of Physics: Conference Series*, 2021, 1986(1): 012003.
[3] H Z Fan, Y F Su, J J Song, et al. Design of "double layer" texture to obtain superhydrophobic and high wear–resistant PTFE coatings on the surface of Al_2O_3/Ni layered ceramics. *Tribology International*, 2019, 136: 455–461.
[4] Z Zhang, W Z Lu, Y F He, et al. Research on optimal laser texture parameters about antifriction characteristics of cemented carbide surface. *International Journal of Refractory Metals and Hard Materials*, 2019, 82: 287–296.
[5] M Wakuda, Y Yamauchi, S Kanzaki, et al. Effect of surface texturing on friction reduction between ceramic and steel materials under lubricated sliding contact. *Wear*, 2003, 254(3–4): 356–363.
[6] I Křupka, M Vrbka, M Hartl. Effect of surface texturing on mixed lubricated nonconformal contacts. *Tribology International*, 2008, 41(11): 1063–1073.
[7] R Rahmani, I Mirzaee, A Sshirvani, et al. An analytical approach for analysis and optimization of slider bearings with infinite width. *Tribology International*, 2010, 43 (8): 1551–1565.
[8] A G Charitopoulos, E E Efstathiou, C I Papadopoulos, et al. Effects of manufacturing errors on tribological characteristics of 3D textured microthrust bearings. *CIRP Journal of Manufacturing Science and Technology*, 2013, 6(2): 128–142.
[9] P Andersson, J Koskinen, S Varjus, et al. Microlubrication effect by laser–textured steel surfaces. *Wear*, 2007, 262(3–4): 369–379.
[10] L J Yang, Y Ding, Bai Cheng, et al. Investigations on femtosecond laser modified micro–textured surface with anti–friction property on bearing steel GCr15. *Applied Surface Science*, 2018, 434: 831–842.
[11] J F Wang, W H Xue, S Y Gao, et al. Effect of groove surface texture on the fretting wear of Ti–6Al–4V alloy. *Wear*, 2021, 486–487: 204079.
[12] P Lu, R J K Wood, M G Gee, et al. A novel surface texture shape for directional friction control. *Tribology Letters*, 2018, 66(1): 1–13.
[13] A Codrignani, D Savio, L Pastewka, et al. Optimization of surface textures in hydrodynamic lubrication through the adjoint method. *Tribology International*, 2020, 148(C): 106352.
[14] Z R Tu, X K Meng, Y Ma, et al. Shape optimization of hydrodynamic textured surfaces for enhancing load–carrying capacity based on level set method. *Tribology International*, 2021, 162: 107136.
[15] W Wang, Y Y He, J Zhao, et al. Optimization of groove texture profile to improve hydrodynamic lubrication performance: Theory and experiments. *Friction*, 2020, 8(1): 83–94.
[16] Z H Shen, F C Wang, Z G Chen, et al. Numerical simulation of lubrication performance on chevron textured surface under hydrodynamic lubrication. *Tribology International*, 2021, 154(3): 106704.
[17] W L Liu, H J Ni, H L Chen, et al. Numerical simulation and experimental investigation on tribological performance of micro–dimples textured surface under hydrodynamic lubrication. *International Journal of Mechanical Sciences*, 2019, 163(C): 105095–105095.
[18] L Y Chen, R T Li, F W Xie, et al. Load–bearing capacity research in wet clutches with surface texture. *Measurement*, 2019, 142: 96–104.
[19] D Li, X F Yang, C Y Lu, et al. Tribological characteristics of a cemented carbide friction surface with chevron pattern micro-texture based on different texture density. *Tribology International*, 2020, 142(C): 106016.
[20] R T Tong, B Han, Z F Quan, et al. Molecular dynamics simulation of friction and heat properties of Nano–texture GOLD film in space environment. *Surface and Coatings Technology*, 2019, 358: 775–784.
[21] Z Y Li, W J Yang, Y P Wu, et al. Role of humidity in reducing the friction of graphene layers on textured surfaces. *Applied Surface Science*, 2017, 403: 362–370.
[22] X Q Hao, W Cui, L Li, et al. Cutting performance of textured polycrystalline diamond tools with composite lyophilic/lyophobic wettabilities. *Journal of Materials Processing Technology*, 2018, 260: 1–8.
[23] D S Xiong, Y K Qin, J L Li, et al. Tribological properties of PTFE/laser surface textured stainless steel under starved oil lubrication. *Tribology International*, 2015, 82: 305–310.
[24] S Wos, W Koszela, P Pawlus, et al. Determination of oil demand for textured surfaces under conformal contact conditions. *Tribology International*, 2016, 93: 602–613.
[25] G Ryk, I Etsion. Testing piston rings with partial laser surface texturing for friction reduction. *Wear*, 2006, 261: 792–796.
[26] K Tønder. Hydrodynamic effects of tailored inlet roughnesses: Extended theory. *Tribology International*, 2004, 37(2): 137–142.
[27] Y Kligerman, I Etsion. Analysis of the hydrodynamic effects in a surface textured circumferential gas seal. *Tribology Transactions*, 2001, 44 (3): 472–478.
[28] A Y Suh, S C Lee, A A Polycarpou. Adhesion and friction evaluation of textured slider surfaces in ultra-low head–disk interface. *Tribology Letters*, 2004, 17: 739–749.
[29] T Y Chen, J H Ji, Y H Fu, et al. Tribological performance of UV picosecond laser multi-scale composite textures for C/SiC mechanical seals: Theoretical analysis and experimental verification. *Ceramics International*, 2021, 47(16): 23162–23180.
[30] K Yagi, W Matsunaka, J Sugimura. Impact of textured surfaces in starved hydrodynamic lubrication. *Tribology International*, 2021, 154: 106756.
[31] L Galda, J Sep, A Olszewski, et al. Experimental investigation into surface texture effect on journal bearings performance. *Tribology International*, 2019, 136: 372–384.
[32] L V Mirantsev, A K Abramyan. Couette flows between various bounding substrates. *Physics Letters A*, 2020, 384(8): 126181.